A&A 390, 13–25 (2002)
DOI: 10.1051/0004-6361:20020737

Astronomy & Astrophysics

High matter density peaks from UVES observations of QSO pairs: Correlation properties and chemical abundances⋆

V. D'Odorico[1], P. Petitjean[1,2], and S. Cristiani[3,4]

[1] Institut d'Astrophysique de Paris, 98bis Boulevard Arago, 75014 Paris, France
[2] LERMA, Observatoire de Paris, 61 Av. de l'Observatoire, 75014 Paris, France
[3] European Southern Observatory, Karl-Schwarzschild-Strasse 2, 85748 Garching, Germany
[4] Osservatorio Astronomico di Trieste, via G.B. Tiepolo, 11, 34131 Trieste, Italy

Received 6 February 2002 / Accepted 15 May 2002

Abstract. We study the transverse clustering properties of high matter density peaks as traced by high column density absorption systems (either Lyman limit systems characterized by $N(\mathrm{H\,I}) \geq 2 \times 10^{17}$ cm^{-2} or C IV systems with $W_r > 0.5$ Å) at redshifts between 2 and 3 with UVES spectra of two QSO pairs (UM680/UM681 at 56 arcsec angular separation and Q2344+1228/Q2343+1232 at 5 arcmin angular separation) and a QSO triplet (Q2139-4433/Q2139-4434/Q2138-4427 at 1, 7 and 8 arcmin angular separation). We find 3 damped Lyman-α systems ($N(\mathrm{H\,I}) \geq 2 \times 10^{20}$ cm^{-2}): 2 coinciding with strong metal systems in the nearby line of sight and 1 matching the emission redshift of the paired QSO; plus 7 Lyman limit systems: 4 forming two matching couples and 3 without a corresponding metal system within ~3000 km s^{-1} in the coupled line of sight. In summary, we detect five out of ten matching systems within 1000 km s^{-1}, indicating a highly significant overdensity of strong absorption systems over separation lengths from ~1 to 8 h^{-1} Mpc. The observed coincidences could arise in gas due to starburst-driven superwinds associated with a quasar or a galaxy, or gas belonging to large scale structures like filaments or sheets. We also determine chemical abundance ratios for three damped Lyman-α systems. In particular, for the damped system at $z \sim 2.53788$ in the spectrum of Q2344+1228, new estimates of the ratios O/Fe, C/Fe are obtained: $-0.02 < [\mathrm{C/Fe}] < 0.06$, $-0.06 < [\mathrm{O/Fe}] < 0.2$. They indicate that O and C are not over-solar in this system.

Key words. galaxies: abundances – galaxies: high-redshift – quasars: absorption lines – cosmology: observations

1. Introduction

Cosmological simulations based on CDM models predict that the *forest* of H I Lyman-α absorption lines, observed in QSO spectra, originates in the fluctuations of the underdense and moderately overdense regions of the intergalactic medium (e.g. Cen et al. 1994; Petitjean et al. 1995; Zhang et al. 1995; Hernquist et al. 1996; Miralda-Escudé et al. 1996; Theuns et al. 1998). The high H I column density systems (Lyman limit and damped Lyman-α systems), on the other hand, arise from radiatively cooled gas in galaxy-sized halos (e.g. Katz et al. 1996).

In the past few years, the association of high column density absorption systems ($N(\mathrm{H\,I}) \gtrsim 10^{16}$ cm^{-2}) with galactic objects has been widely verified at redshifts up to $z \sim 1$, by direct imaging of QSO fields and follow-up spectroscopy. The observed impact parameters for galaxies giving rise to Mg II absorption systems suggest the presence of extended gaseous halos of spherical geometry and radii $R \sim 50\,h^{-1}$ kpc (where h is the Hubble constant in units of 75 km s^{-1} Mpc^{-1}, and $q_0 = 0$) (Bergeron & Boissé 1991; Bergeron et al. 1992; Steidel et al. 1994; Guillemin & Bergeron 1997). While damped Lyman-α systems (DLASs) are likely due to smaller structures (Wolfe et al. 1992; Le Brun et al. 1997).

The correlation properties of absorbers along the line of sight (LOS) were studied recently. A trend of increasing correlation signal with increasing H I column density at $z \sim 2$ is detected for QSO absorption lines up to $N(\mathrm{H\,I}) \sim 10^{17}$ cm^{-2} (Cristiani et al. 1997). At the same redshift, higher column density systems are expected to be more correlated according to the hierarchical clustering scenario, as they are believed to be associated with galactic or proto-galactic structures. The classic approach to compute the correlation function is complicated by their rareness. In the hypothesis that DLASs are indeed galaxies, Wolfe (1993) handles this problem by comparing the density of Lyman-α emitters in the field and at the redshift of observed DLASs ($< z > = 2.6$), with that of randomly chosen fields at similar redshift. A Poissonian distribution of galaxies in the fields centred on DLASs is ruled out with more than 99.5% confidence, but little else can be said on the correlation function.

Close pairs or groups of QSO LOSs represent an alternative, efficient tool to investigate the correlation properties of absorbers. Francis & Hewett (1993) find two candidate DLASs

Send offprint requests to: V. D'Odorico,
e-mail: dodorico@ts.astro.it

⋆ Based on material collected with the European Southern Observatory Very Large Telescope operated on Cerro Paranal (Chile). Proposals 65.O-0299 and 67.A-0078.

Table 1. Journal of observations September 2000.

Object	Mag	z_e	Wvl. range (nm)	t_{exp} (sec)
UM680	18.6	2.144	305–387 / 477–680	7950
UM681	19.1	2.122	305–387 / 477–680	11 600
Q2344+1228	17.5	2.773	376–498 / 670–10^3	3600
Q2343+1232	17.00	2.549	376–498 / 670–10^3	3600
Q2139-4433	20.18	3.220	413–530 / 559–939	9000
Q2139-4434	17.72	3.23	413–530 / 559–939	7200

Table 2. Adopted solar abundances for the relevant chemical elements.

H	Hydrogen	0.00
C	Carbon	−3.45
N	Nitrogen	−4.03
O	Oxygen	−3.13
Si	Silicon	−4.45
S	Sulphur	−4.79
Fe	Iron	−4.49

in the spectrum of Q2138-4427 at $z_a \simeq 2.38$ and 2.85 matching in redshift two weaker Lyman-α absorptions in the spectrum of the companion quasar Q2139-4434, at a separation of 8 arcmin on the plane of the sky. Later deep imaging of the field of Q2139-4434 has indeed confirmed the presence of a group of red, radio quiet galaxies at $z \simeq 2.38$. This galaxy cluster, with mass $\gg 3 \times 10^{11}\ M_\odot$, could have collapsed before redshift 5 (Francis et al. 1996, 1997, 2001a).

In this paper, we use two QSO pairs and a triplet to analyse the correlation behaviour of high matter density peaks. We assume that *high matter density peaks* are traced by optically thick absorbers (i.e. with column density $N(\mathrm{H\,I}) \gtrsim 2 \times 10^{17}$ cm^{-2}) and by strong metal systems (characterised by C IV rest equivalent width $W_r(\lambda 1548) \geq 0.5$ Å).

The structure of the paper is the following: Sect. 2 describes the observations and data reduction of 6 new UVES spectra of three QSO pairs (Q2344+1228 and Q2343+1232, UM680 and UM681, Q2139-4433 and Q2139-4434); in Sect. 3, we describe in more detail one sub-damped and two damped Lyman-α systems detected in the spectra, with a particular attention to chemical abundances. Section 4 is dedicated to the description of the observed coincidences. The discussion is reported in Sect. 5 and the summary of results in Sect. 6.

All through the paper, we adopt a cosmology with $q_0 = 0.5$ and $h = H_0/75$ km s^{-1} Mpc^{-1}. Spatial separations are always *comoving*.

2. Observations and data reduction

In September 2000, we obtained high resolution spectra of three QSO pairs with the UV and Visual Echelle Spectrograph (UVES, Dekker et al. 2000) mounted on the Kueyen telescope of the ESO VLT (Cerro Paranal, Chile). The journal of observations is reported in Table 1.

Spectra were taken in dichroic mode with a slit of 1.2″ and binning of 2×2 pixels. A binning of 3×2 pixels was adopted for one of the spectra of the faintest object Q2139-4433. The resolution is ∼37 000 and ∼35 000 in the blue and in the red portion of the spectra respectively. Wavelength ranges in the blue arm were chosen in order to cover most of the Lyman-α forest of each object. Another paper will be devoted to the detailed discussion of the lines in this region (D'Odorico et al. in preparation).

Data reduction was carried on by using the specific UVES pipeline (see Ballester et al. 2000) in the framework of the 99NOV version of the ESO reduction package, MIDAS. The continuum was determined by manually selecting regions not affected by evident absorption and by interpolating them with a spline function of 4th degree.

Metal absorption systems were detected, in general, by first identifying C IV or Mg II doublets and then looking for other ionic transitions at the same redshift. Atomic parameters for the lines were taken from Verner et al. (1994). New oscillator strengths were adopted for most of the Fe II transitions (Bergeson et al. 1994, 1996; Raassen & Uylings 1998). Lines were fitted with Voigt profiles in the LYMAN context of the MIDAS reduction package. The reported errors on column densities are the $1\,\sigma$ errors of the fit computed in MIDAS. They possibly underestimate the real error on the measure since they do not take into account the uncertainty on the continuum level determination. Furthermore, they are the result of a single fitting model which is not univocal in certain column density regimes and for heavily blended systems (Fontana & Ballester 1995). In the cases in which the column density was weakly constrained and the MIDAS procedure could not converge to a unique solution (e.g. for saturated H I Lyman-α lines), indicative values of the column density were obtained by use of the interactive fitting program XVoigt (Mar & Bailey 1995).

We could analyse also the UVES spectrum of Q2138-4427 ($B = 18.9$, $z_e \simeq 3.17$), with similar resolution and wavelength coverage. The detailed description of its reduction and of the two DLASs present in it, will be given elsewhere (Ledoux et al. in preparation).

3. Properties of the main absorption systems

In the following, we briefly discuss the relative abundances of some chemical elements for two DLASs and a sub-DLAS detected in the present spectra. All the abundances are given relative to the solar values of Grevesse & Anders (1989) and Grevesse & Noels (1993), in the notation $[X/Y] = \log(X/Y)_{\rm obs} - \log(X/Y)_\odot$ (see Table 2). A summary of the obtained chemical abundances is reported in Table 3.

3.1. The sub-DLAS at $z_a \sim 1.788$ in UM681

This is a newly detected metal absorption system. The H I Lyman-α absorption at this redshift shows a clear Lorentzian wing on the blue side of the velocity profile (see Fig. 1). In order to obtain an estimate of the H I column density, we fit the profile with two components at the redshifts of the two

Table 3. Measured relative chemical abundances. If not otherwise stated the error on the logarithmic column densities and on the relative abundances is 0.1.

Object	Redshift	Δv^a	log N(H I)^b	[Fe/H]	[Si/H]	[N/H]	[S/H]	[N/S]	[C/Fe]	[0/Fe]
UM681	1.78745	−150.5	18.6			−0.6 ± 0.2	−0.3 ± 0.2			
Q2343+1232	average^c		20.35	−1.2 ± 0.2		−1.1	−0.7			
	2.43125	0.0						−0.3		
Q2344+1228	average^c		20.4	−1.8 ± 0.2	−1.85	−2.75				
	2.53746	−35.6							<0.06	<0.2

[a] Relative velocities as reported in the corresponding figures.
[b] Since it is not possibile to disentangle the velocity structure of the H I Lyman-α absorption lines, the profiles have been fitted with one or two components at the redshift of the stronger components observed in the neutral and singly ionised absorption lines.
[c] Average value obtained considering the sum of the column densities of all the components of the iron absorption profile.

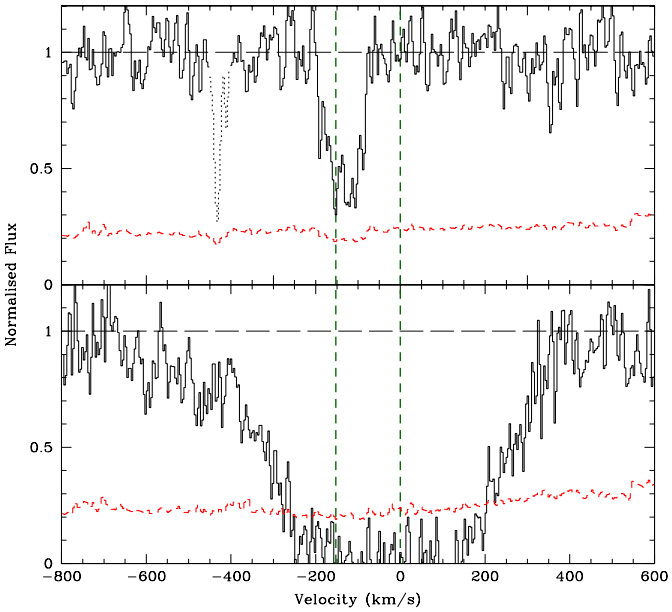

Fig. 1. $z \sim 1.788$ – coincidence between the sub-damped Lyman-α absorption line at $z_a \simeq 1.788$ in the spectrum of UM681 (bottom panel) and a weak Lyman-α absorption line ($\log N(\mathrm{H\,I}) \simeq 13.81 \pm 0.05$) in the spectrum of UM680 (top panel). The spatial separation between the two LOSs at this redshift is ~870 h^{-1} kpc. The dotted lines mark the position of the 2 components fitting the sub-DLAS at redshifts $z_a = 1.78745$ and 1.78885 (origin of the velocity axes).

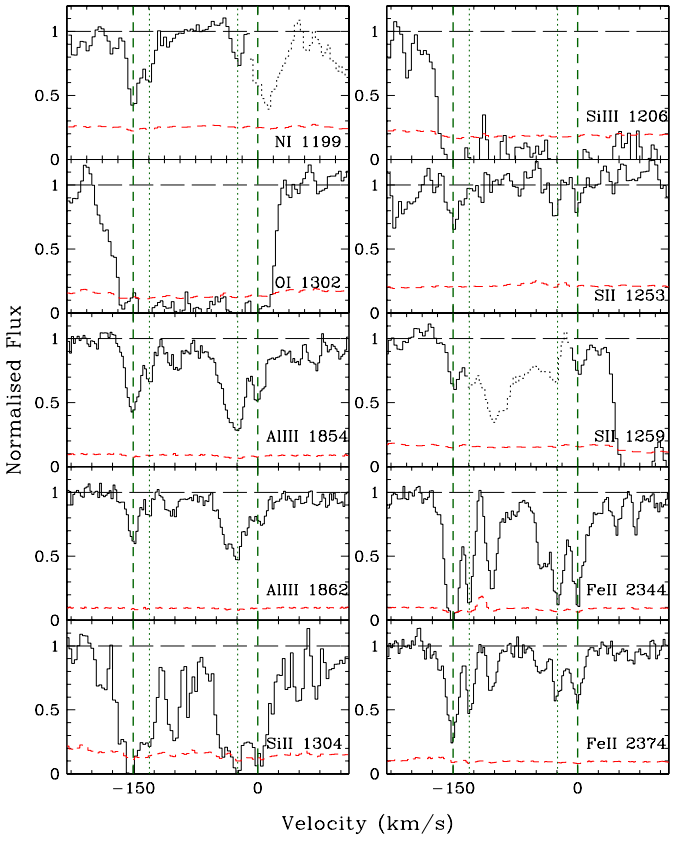

Fig. 2. UM681: ionic transitions of the system at $z_a \simeq 1.788$. The dotted vertical lines mark the position of the components discussed in the text. The two thick, dashed lines corresponds to the redshifts of the two components used to fit the H I Lyman-α absorption.

strongest groups of lines seen in the singly ionised element profiles (see Fig. 2). At $z_a \simeq 1.78745$ ($v \simeq -150$ km s^{-1} in the figures), we measure a column density $\log N(\mathrm{H\,I}) \sim 18.6 \pm 0.1$ and at $z_a \simeq 1.78885$ ($v \simeq 0$ km s^{-1}), $\log N(\mathrm{H\,I}) \sim 19.0 \pm 0.1$. The associated heavy element transitions have a complex structure spread over about 250 km s^{-1} with at least 8 narrow components in Fe II, Si II and Al III and 4 components in N I and S II (see Fig. 2). O I, C II and Si III are either saturated or blended, Si IV, C IV and Al II are outside our wavelength range.

The observed H I column density is not high enough to assure that no ionisation corrections have to be applied to get the relative chemical abundances (see e.g. Viegas 1995). We derive an indicative measure of the nitrogen and sulphur abundances by using the Cloudy software package (Ferland 1997) to build a photoionisation model and estimate the ionisation corrections. We consider the UV background flux due to quasars and galaxies (Madau et al. 1999) and try to recover the observed column densities of the components at $z_a \simeq 1.78745$ and 1.78765 ($v \simeq -150$ and -130 km s^{-1} in Fig. 2). The results do not change significantly if we adopt an ionizing spectrum due to a single stellar population of solar metallicity and 0.1 Gyr. The resulting ionisation corrections are ~2.3, 0.2 and 14 to be multiplied for the ratios N I/H I, S II/H I and N I/S II respectively. Since the corrections are relatively small in the first two cases,

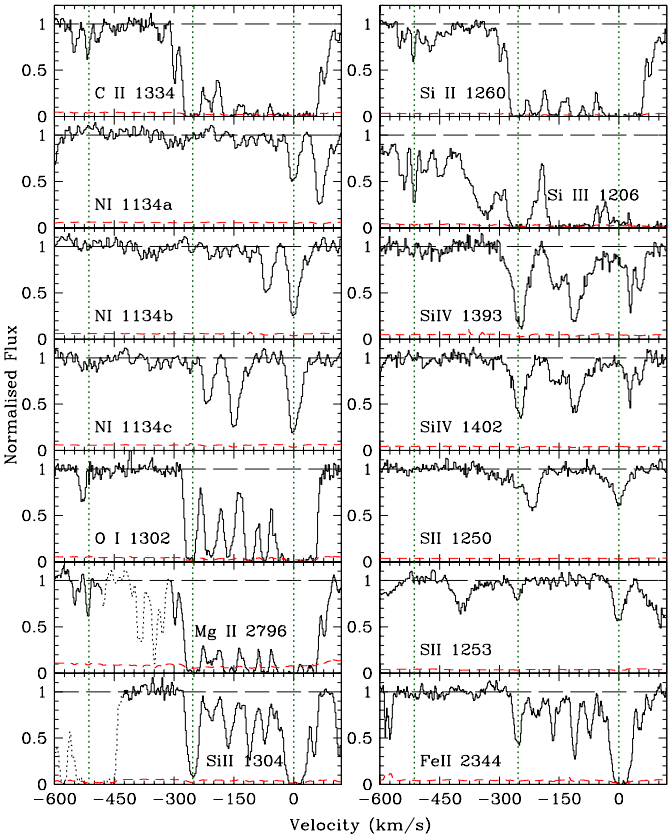

Fig. 3. Q2343+1232: ionic transitions associated to the DLAS at $z_a \simeq 2.43125$. The dotted line at the extreme left marks the position of the satellite sub-system at $z_a = 2.42536$ (see text). The dotted lines on the right are drawn at the redshifts $z_a = 2.42834$ and 2.43125 (origin of the velocity axes) of the components discussed in the text.

we compute the corresponding abundance ratios. N I λ 1199 is partially blended (see Fig. 2), thus we estimate the nitrogen abundance from the two components at lower redshift ($v \simeq -150$ and -130 km s^{-1} in Fig. 2), associated with the $z_a \simeq 1.78745$ H I component with $\log N(\mathrm{H\,I}) \simeq 18.6 \pm 0.1$. From this we derive [N/H] $\simeq -0.6 \pm 0.2$ corrected for the ionisation. This value is about one order of magnitude larger than the higher value measured in DLASs published in the literature (Centurión et al. 1998; Lu et al. 1998). The corrected sulphur abundance ratio for the same components is [S/H] $\sim -0.3 \pm 0.2$ which again is about one order of magnitude larger than what is observed in DLASs.

These measurements, although slightly uncertain, suggest that sub-DLAS could have higher metal abundances than DLASs, as already observed in LLS (e.g. D'Odorico & Petitjean 2001), and probe a more evolved chemical stage of high redshift galaxies when gas has been partly consumed by star formation.

3.2. The DLAS at $z_a \simeq 2.43125$ in Q2343+1232

This DLAS, as well as the one seen along the LOS of Q2344+1228 (see next section), has first been detected by Sargent (1987). The two QSOs were observed recently with HIRES+Keck and the relative chemical abundances of the two systems were used in statistical samples (Rauch et al. 1997; Lu et al. 1998; Prochaska & Wolfe 1998, 2001; Prochaska et al. 2001).

The metal absorption complex corresponding to this damped system is made of two groups of lines. The major one counts at least 8 components, with the strongest one at $z_a \simeq 2.43125$ ($v = 0$ km s^{-1} in Fig. 3). This component is heavily saturated in C II, O I, Mg II, and Si II. It shows absorption due to the two triplets of N I, λ 1134 Å and λ 1200 Å, and to the S II triplet, $\lambda\lambda\lambda$ 1250, 1253, 1259 Å. The Si IV doublet is clearly identified in this complex, the C IV doublet is outside our spectral range but was detected by Sargent et al. (1988). A satellite sub-system is observed at more than 500 km s^{-1} from the centre of the main one, at $z_a \simeq 2.42536$. It is very weak and shows transitions due to C II, Mg II, Si II and Si III.

Since we cannot disentangle the velocity structure of the hydrogen absorption, we assume a single component at the redshift of the strongest component observed in singly ionised lines at $z_a \simeq 2.43125$. The total H I column density is $\log N(\mathrm{H\,I}) \simeq 20.35 \pm 0.05$ and the error is mainly due to the uncertainty in the position of the continuum. The average iron abundance is [Fe/H] $\simeq -1.2 \pm 0.2$. While, we obtain [S/H] $\simeq -0.7 \pm 0.1$ and [N/H] $\simeq -1.1 \pm 0.1$. Those estimates are $\sim$0.2 and 0.5 dex higher respectively, than those reported by Lu et al. (1998). The difference for sulphur is within the uncertainties (at the 3 σ level), while the larger one for nitrogen could be due to the fact that Lu et al. (1998) used the saturated N I triplet at λ 1200 Å.

As previously stated, the main component is badly saturated for all the observed transitions due to C, O and Si, so relative abundances for these elements cannot be determined. On the other hand, we can study the abundance ratios of S, N and Fe at this redshift, assuming that ionisation corrections are negligible. This hypothesis is supported by the large column density characterising this component and by the absence of Si IV absorption. We measure column densities: $\log N(\mathrm{S\,II}) \simeq 14.75 \pm 0.05$, $\log N(\mathrm{N\,I}) \simeq 15.16 \pm 0.05$ (where we do not consider the N I triplet at λ 1200 Å because it is saturated and affected by the wing of the damped H I Lyman-α line) and $\log N(\mathrm{Fe\,II}) \simeq 14.49 \pm 0.08$. From which we derive the abundance ratios: [S/Fe] $\simeq 0.6 \pm 0.1$, and [N/S] $\simeq -0.3 \pm 0.1$. The latter abundance ratio, which is not affected by dust, can be compared with the ratios [N/O] measured for metal poor Galactic stars making the assumption, [S/O] $\equiv 0$ as reported by Centurión et al. (1998). Our measurement is larger than any other for DLASs present in the literature (see also Lu et al. 1998) and it is consistent with values obtained for H II regions in dwarf galaxies.

The strong Si IV absorption imply that ionisation corrections could be necessary to determine the abundance ratios in the other components of the system. Nothing can be said on the H I column density corresponding to the single components. This makes hard the realization of a photoionisation model to determine the ionisation corrections. We report the measured column densities of sulphur and nitrogen (a faint absorption is observed for the transition N I λ 1200) relative to the component at $z_a \simeq 2.42834$ ($v \simeq -250$ km s^{-1} in Fig. 3), $\log N(\mathrm{S\,II}) \simeq 14.22 \pm 0.05$ and $\log N(\mathrm{N\,I}) \simeq 13.5 \pm 0.05$.

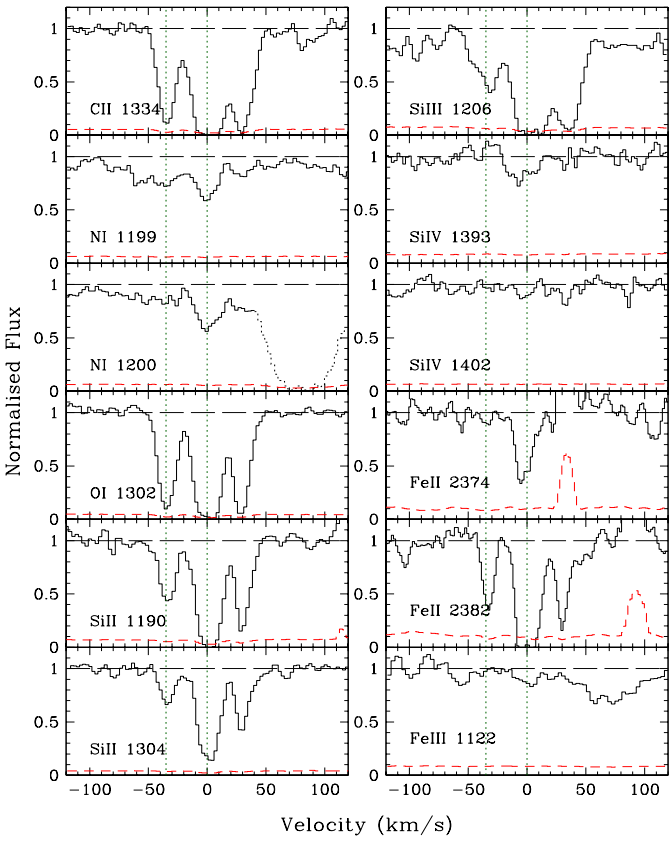

Fig. 4. Q2344+1228: ionic transitions associated to the DLAS at z_a = 2.53788 (origin of the velocity axes). The left dotted line marks the position of the component at z_a = 2.53746 discussed in the text.

3.3. The DLAS at $z_a \simeq 2.53788$ in Q2344+1228

The damped H I Lyman-α absorption line of this system has been fitted with a single component at the redshift of the strongest component observed in the neutral and singly ionised lines of associated heavy elements ($z_a \simeq 2.53788$). The H I column density is $\log N(\mathrm{H\,I}) \simeq 20.4 \pm 0.1$, where the error on the column density is due mainly to the positioning of the continuum level.

In Fig. 4, we show the ionic transitions observed for the DLAS. The C IV doublet is outside our wavelength range and it was not observed in the low resolution spectrum by Sargent et al. (1988). The iron and silicon column densities can be derived from non saturated lines to obtain the average values, [Fe/H] $\simeq -1.8 \pm 0.2$, and [Si/H] $\gtrsim -1.85 \pm 0.1$. While, [N/H] $\simeq -2.75 \pm 0.11$, which is in good agreement with the value found by Lu et al. (1998).

The absence of high ionisation lines and the simple velocity profile of the system allow the assumption that ionisation corrections are negligible in this case. We can thus obtain reliable abundance ratios from the column densities of the transitions observed in the single components.

N I is observed in the central component, we compute the abundance ratio [N/Fe] $\simeq -0.8 \pm 0.1$, which is consistent with previous measurements for DLAS. The central component is unusable to derive reliable abundance measures for other chemical elements because all the observed lines are heavily saturated.

In the component at lower redshift ($z_a \simeq 2.53746$, $v \simeq -35.6$ km s^{-1} in Fig. 4), the ratio [Si III/Si II] $\simeq -0.66 \pm 0.07$ implies that ionisation corrections are small at this velocity. We observe transitions due to Si II and Fe II that are not saturated, from which the relative abundance [Si/Fe] $\simeq 0.2 \pm 0.1$ is obtained. On the other hand, C II and O I are slightly saturated but not going to zero, this results in the upper limits: $-0.02 <$ [C/Fe] < 0.06 and $-0.06 <$ [O/Fe] < 0.2. Reliable measures of O and C abundances are quite rare. We discuss the implications of our result in the following section.

3.4. Comments on the measures of [O/Fe] and [C/Fe]

α-capture elements are mainly produced by type II SNe which should dominate in the early stages of the chemical evolution of galaxies, while type I SNe contribute iron peak elements later on. Therefore, the [α/Fe] abundance ratio can be used to trace the chemical evolution history and, to a certain extent, the nature of galaxies. Oxygen and sulphur are more reliable estimators of α-element abundances than silicon which is subject to dust depletion. Abundance studies of carbon (e.g. Tomkin et al. 1995) indicate that in the disk of our Galaxy [C/Fe] and [α/Fe] show similar trends with [Fe/H].

Measures of C and O in DLASs are generally complicated by the fact that often the only available lines are C II λ 1334 and O I λ 1302 which most of the times are heavily saturated. In the DLAS described in Sect. 3.3, we constrain the values of the O/Fe and C/Fe ratios, considering a single component which is only mildly saturated and not going to zero. We derive that the C/Fe ratio is consistent with solar while the O/Fe and Si/Fe ratios are consistent among them and show a very small enhancement. The average iron abundance of the system is about 1/100 solar. Our result, together with the recent measures by Molaro et al. (2000) for the DLAS in the spectrum of Q0000-26, indicates that there is no evidence for the [O/Fe] ratio to be over-solar in DLAS. This is at a variance with what is observed in the atmosphere of Galactic stars at the same metallicity (but see also Dessauges-Zavadsky et al. 2001).

The abundance pattern which is closest to the above data is that of an old starburst, as is observed at the boundaries of our galactic disk, although, in general, for larger iron abundances (Chiappini et al. 1999).

4. Coincidences of high matter density peaks

In this section, we describe the observed pairs of quasars and list the absorption systems with $N(\mathrm{H\,I}) \gtrsim 2 \times 10^{17}$ cm^{-2} found in the 7 spectra. For each of the systems, we search the adjacent line of sight for the presence of any absorption at the same redshift. When a LLS or a C IV system with rest equivalent width $W_r > 0.5$ Å is seen along the second LOS within $\sim$1000 km s^{-1} from the former LLS, we call this a coincidence. The observed number densities of LLS and C IV absorption systems with $W_r > 0.5$ Å are similar at the same redshift (e.g. Steidel et al. 1988; Steidel 1990). We can therefore assume that they trace the same kind of overdensity.

The numbers associated with the coincidences correspond to those in Table 4 and Fig. 15.

4.1. The QSO pair UM680 and UM681

These two QSOs (also called Q0307-195A,B) are separated by 56 arcseconds on the plane of the sky, corresponding to ~830–940 h^{-1} kpc in the considered redshift interval. Spectra at low and intermediate resolution of this pair have been used in the past to study the correlation of C IV and Lyman-α forest lines (Shaver & Robertson 1983; D'Odorico et al. 1998).

1) $z \simeq 1.788$ – there is no metal system along the LOS of UM680 corresponding to the sub-DLAS at $z_a \simeq 1.788$ observed in the spectrum of UM681 (see Sect. 3.1). A weak Lyman-α absorption, $\log N(\mathrm{H\,I}) \simeq 13.81 \pm 0.05$, is observed at $z_a \simeq 1.7876$ (see Fig. 1). From the observed number density of H I Lyman-α absorption lines with column density in the range $13.1 \leq \log N(\mathrm{H\,I}) \leq 14$ (Kim et al. 2001), the probability for such an absorption to fall in a velocity bin of 200 km s^{-1} at this redshift is $\mathcal{P} \sim 0.3$–0.4.

2) $z \simeq 2.03$ – the coincident systems observed at $z_a \simeq 2.03520$ and $z_a \simeq 2.03215$ in the spectra of UM680 and UM681 respectively, are two candidate LLSs which show absorption lines due to the same ionic transitions with a shift of ≃300 km s^{-1} (see Fig. 5). We detect low ionisation absorption lines due to Al II, Si II and Fe II, together with Al III, Si III and Fe III, the latter only in UM680. The corresponding Si IV and C IV absorption doublets are outside our wavelength coverage, but their presence is discussed in Shaver & Robertson (1983).

It is not possible to constrain the value of the H I column density of both systems due to the complexity of the profile. The Lyman-β lines are in a region of the spectrum with low signal-to-noise ratio and probably blended. From the equivalent width ratio of Si II and Fe II to C IV (as measured by Shaver & Robertson 1983) we derive that the systems are likely in a low excitation state and have $N(\mathrm{H\,I}) > 10^{18}$ cm^{-2} (see Bergeron & Stasińska 1986).

3) $z \simeq 2.122$ – the QSO UM681 presents a metal system at its emission redshift ($z_a \simeq 2.12209$) with lines due to C IV, N V, O VI and S IV and also weak low ionisation lines (see Fig. 6). This system, although characterized by highly ionised transitions, has a velocity spread of less than ~250 km s^{-1} and does not show any evidence of partial coverage. Furthermore, the presence of singly ionised absorption lines and the symmetric velocity profile favour an absorber with a dense core. Therefore, although the system is located in the vicinity of the quasar it is probably not associated with it.

In addition, there is a very similar absorption system along the LOS of UM680, at $z_a \simeq 2.12312$, corresponding to a velocity shift of ~100 km s^{-1} (see Fig. 6). The transverse spatial separation between the two LOSs at this redshift is ~940 h^{-1} kpc. The latter system is located at ~2000 km s^{-1} from the emission redshift of UM680; the same arguments as before are valid to reject the hypothesis that this is due to gas associated with either of the two quasars. The observed H I Lyman-α and Lyman-β absorption lines for this system are consistently fitted with a main component of column density $\log N(\mathrm{H\,I}) \gtrsim 17.3$.

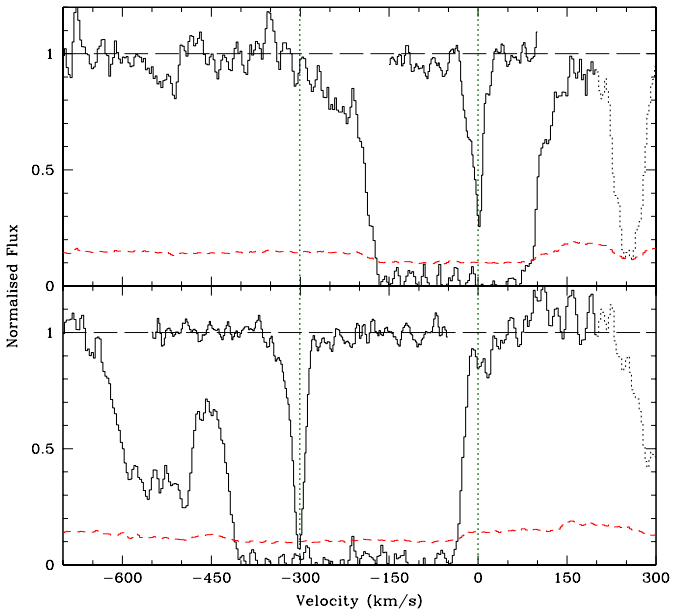

Fig. 5. $z \sim 2.03$ – coincident absorption systems in the spectra of UM680 (top panel) and UM681 (bottom panel). The H I Lyman-α transitions are shown with superposed the corresponding Al II λ 1670 one. The transverse spatial separation between the two LOSs at this redshift is ~924 h^{-1} kpc. The dotted lines mark the position of the metal lines at $z_a = 2.03215$ and $z_a = 2.03520$ (origin of the velocity axes).

Figure 7 shows the H I Lyman-α emission region in the two QSO spectra. The coinciding Lyman-α absorptions at $z_a \sim 2.122$ are shown, together with the associated N V λ 1238 lines (the N V λ 1242 transitions fall outside the observed wavelength range). Another pair of Lyman-α absorptions is observed at $z_a \sim 2.099$, which shows an associated N V doublet in the spectrum of UM680, while does not have any detected associated metal line in UM681.

Shaver & Robertson (1983) suggest the existence of a uniform, 1 Mpc diameter, gaseous disk associated with UM681 to explain the coincidence at $z_a \sim 2.122$. The presence of a further coincidence at ~2000 km s^{-1} from this one, favours the thesis that the absorptions are due to a coherent gaseous structure embedding both quasars and possibly small galactic objects. Deep imaging of the field could possibly shed light on the nature of the absorbers and of the ionising processes at work in the gas.

4.2. The QSO pair Q2344+1228 and Q2343+1232

The first spectra of this QSO pair were presented by Sargent et al. (1988), the two objects are separated by 5 arcmin on the plane of the sky, corresponding to a transverse spatial separation of ≃5 h^{-1} Mpc in the considered redshift range. The remarkable feature is the presence of a DLAS in each of the LOS (see Sect. 3).

The emission redshift of Q2343+1232 reported by Lu et al. (1998), $z_e \simeq 2.549$, is consistent with the position of the emission lines observed in the Sargent et al. (1988) spectrum

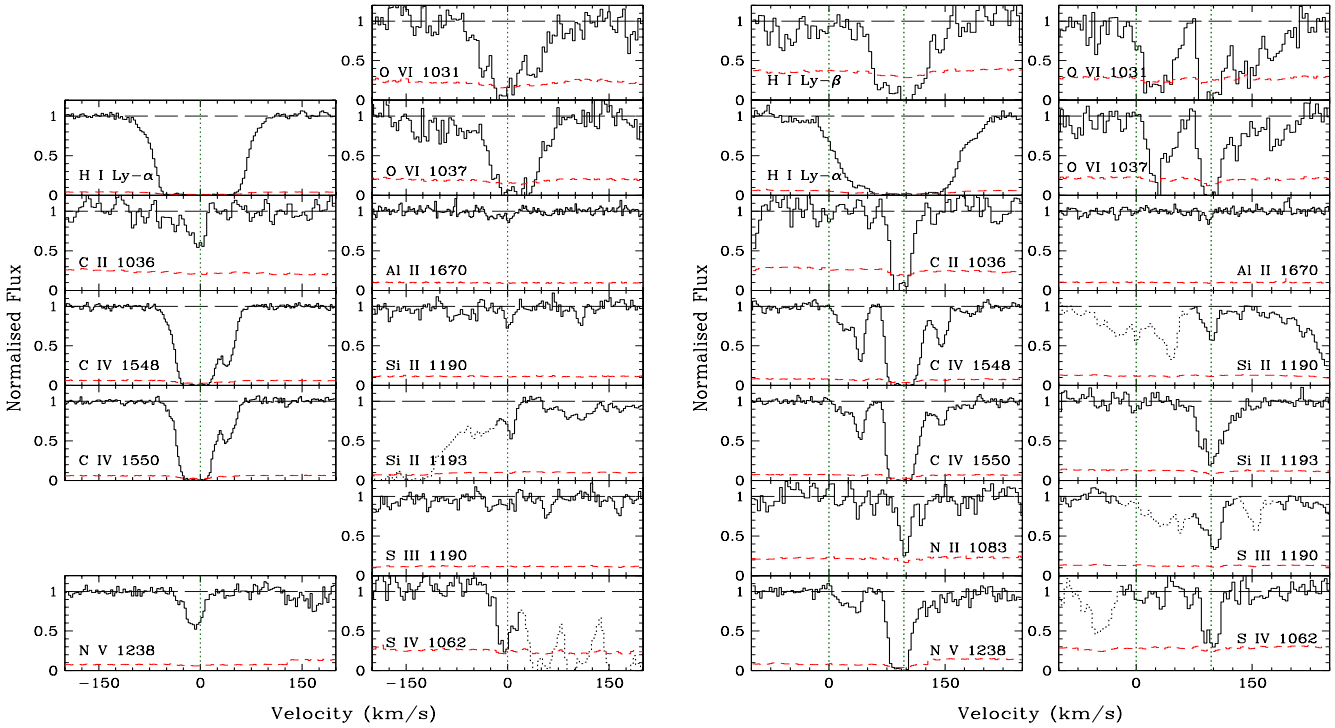

Fig. 6. Left: ionic transitions observed at $z_a = 2.12209$ (origin of the velocity axes) in the spectrum of UM681. This redshift is obtained from the fitting of the low ionisation lines; the center of the velocity profile of the high ionisation lines, determined by the N v λ1238 Å transition, is shifted by $\simeq -8.5$ km s^{-1}. Right: ionic transitions observed at $z_a = 2.12312$ ($v \simeq 97$ km s^{-1}) in the spectrum of UM680. The origin of the velocity axes is kept at $z_a = 2.12209$, redshift of the low ionisation transitions observed in the coincident system in the spectrum of UM681. The transverse separation between the two LOSs at this redshift is ~940 h^{-1} kpc.

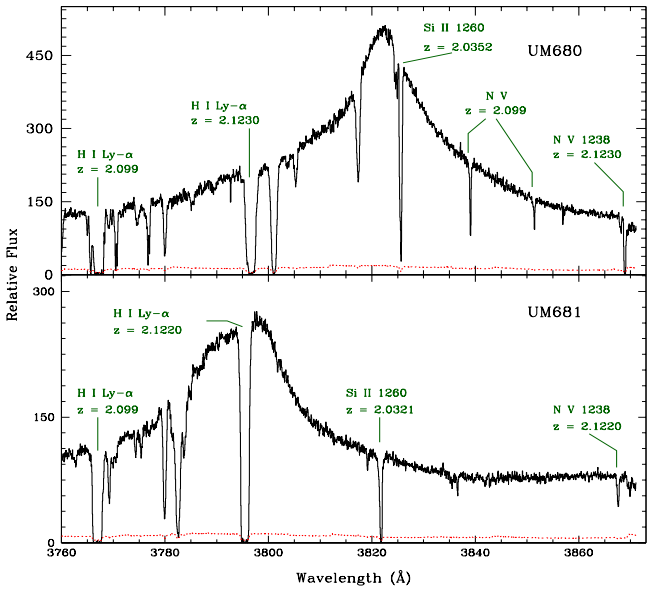

Fig. 7. Lyman-α emission region in the spectra of the QSOs UM680 (top panel) and UM681 (bottom panel). Marked are the two coinciding H I Lyman-α lines at $z_a \simeq 2.099$ and 2.122 and other interesting metal absorption lines (see text). The two LOSs are separated by ~940 h^{-1} kpc at $z = 2.122$.

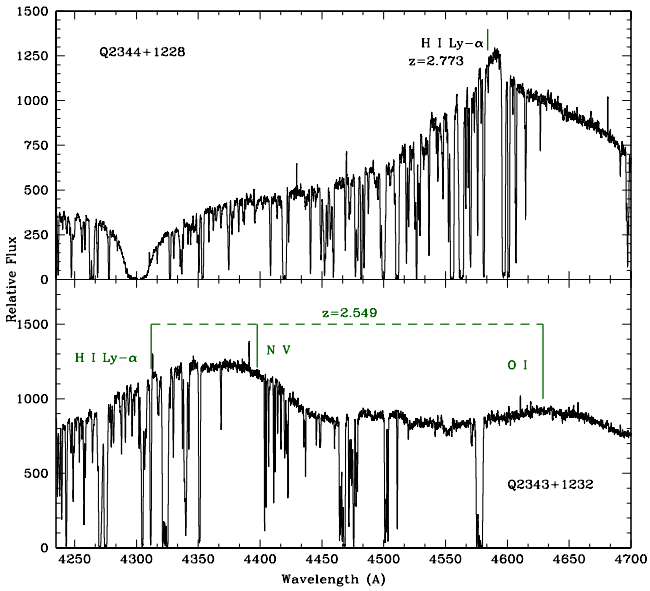

Fig. 8. H I Lyman-α emission regions in the spectra of Q2344+1228 (top panel) and Q2343+1232 (bottom panel). The transverse spatial separation between the two LOSs in this region is ~5 h^{-1} Mpc. The dashed vertical lines mark: in the top panel, the position of the H I Lyman-α emission at $z_e = 2.773$; in the bottom panel, the labeled emission lines at $z_e = 2.549$, with the shifted rest wavelengths by Tytler & Fan (1992).

(Si IV+O IV] and C IV) and with the O I emission in our spectrum (marked in Fig. 8), when the shifted rest wavelengths computed by Tytler & Fan (1992) are used. Likely, the peak observed at $\lambda \sim 4375$ Å is partly due to the N v emission, while the maximum of the Lyman-α emission is strongly absorbed.

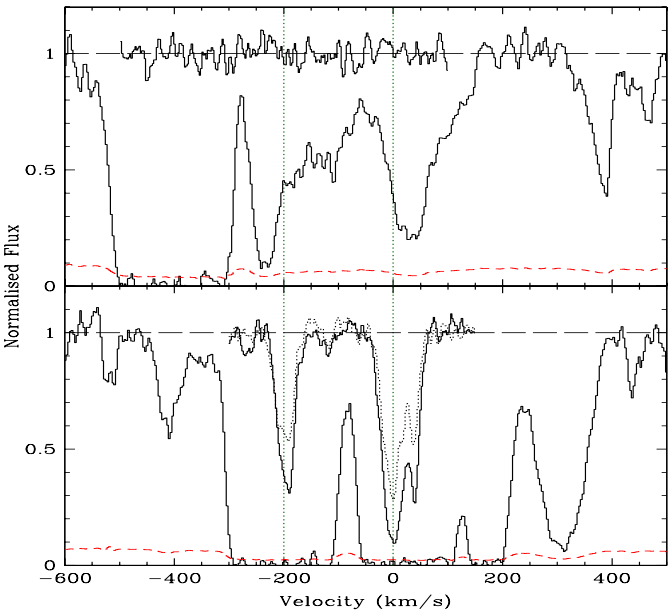

Fig. 9. $z \sim 2.171$ – coincidence between the LLS at $z_a \simeq 2.17115$ (origin of the velocity axes) in the spectrum of Q2343+1232 (bottom panel) and a H I Lyman-α absorption without associated metals in the spectrum of Q2344+1228 (top panel). Overplotted on the Lyman-α absorptions are the corresponding C IV λ 1548 and λ 1550 spectral regions showing a detectable absorption only in Q2344+1232. The two LOSs are separated by 5 h^{-1} Mpc.

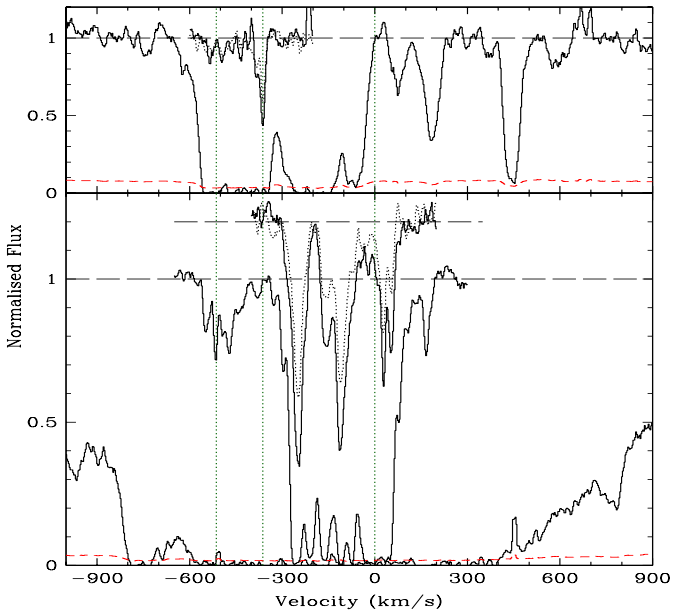

Fig. 10. $z \sim 2.43$ – coincident absorption systems in the spectra of Q2344+1228 (top panel) and Q2343+1232 (bottom panel). The two LOS are separated by ~5.3 h^{-1} Mpc. The H I Lyman-α transitions are shown with superposed: the corresponding Si IV doublet at $z_a = 2.4271$ (top) and the Si II λ 1260 plus the Si IV doublet shifted upward by 0.2 for clearness (bottom). The dotted vertical lines mark from left to right: the position of the weak metal complex in Q2343+1232 at $z_a = 2.42536$, the main component of the metal absorption in Q2344+1228 and the main component of the low ionisation metal lines in Q2343+1232 at $z_a = 2.43125$ (origin of the velocity axes).

We identify two absorption systems at $z_a > z_e$: a N V doublet and the corresponding Lyman-α absorption at $z_a \simeq 2.5698$ ($\Delta v \simeq 1750$ km s^{-1}), together with another possible Lyman-α line at $z_a \simeq 2.579$ ($\Delta v \simeq 2500$ km s^{-1}). They do not show any signature of partial coverage and they could be explained by the presence of a cluster of galaxies of which the QSO itself is a member (e.g. Weymann et al. 1979).

4) $z \simeq 2.171$ – in the spectrum of Q2343+1232, we identify a metal system at $z_a \simeq 2.171$ which could be a LLS on the ground of the column density ratios of the observed transitions (Bergeron & Stasińska 1986). In particular, O I/C IV ~ 0.6, Mg II/C IV ~ 0.4 and Si II/Si IV ~ 3.7. No metal system is detected along the companion LOS within ~3000 km s^{-1}. However, a complex H I Lyman-α absorption is present (see Fig. 9) whose velocity profile appears to match that of the Lyman-α in Q2343+1232 when shifted red-ward by ~240 km s^{-1}.

5) $z \simeq 2.43$ – in the spectrum of Q2343+1232, the DLAS at $z_a \simeq 2.43$ (see Sect. 4.2) coincides with a metal system at $z_a \simeq 2.4271$ (redshift of the Si IV main component) in the companion LOS, showing only high ionisation lines (C IV was detected by Sargent et al. 1988) and a strongly saturated Lyman-α ($W_r \simeq 2$ Å) (see Fig. 10). The H I absorption is likely not a LLS since singly ionised lines are not detected (like Mg II and Fe II). An acceptable fit of the profile is obtained with two main components at N(H I) ~ 10^{15} and ~6.3×10^{15} cm^{-2}, which however should be considered as lower limits.

6) $z \simeq 2.54$ – the DLAS at $z_a \simeq 2.53788$ in the spectrum of Q2344+1228 (see Sect. 4.1) does not have a corresponding metal system on the LOS to Q2343+1232, but it is indeed at ~940 km s^{-1} from the H I Lyman-α emission at the redshift of this quasar (see Fig. 8).

4.3. The QSO triplet Q2138-4427, Q2139-4433 and Q2139-4434

The quasar Q2139-4434 ($z_e = 3.23$) was observed at intermediate resolution together with its companion Q2138-4427 ($z_e = 3.17$) by Francis & Hewett (1993). They are separated by 8 arcmin on the plane of the sky. Francis and Hewett observed common strong Lyman-α absorptions at $z \sim 2.38$ and $z \sim 2.85$ and further imaging of the field revealed the presence of a cluster of galaxies at $z \sim 2.38$ (Francis et al. 1996, 1997, 2001a). Wolfe et al. (1995) confirmed the damped nature of the system at $z \sim 2.85$ in the spectrum of Q2138-4427. We obtained high resolution spectra of Q2138-4427, Q2139-4434 and of Q2139-4433 ($z_e = 3.220$, $R = 19.97$; Hawkins & Véron 1996). The latter two QSOs are separated by 1 arcmin on the plane of the sky.

7) $z \simeq 2.38$ – the strong Lyman-α absorption at $z_a \simeq 2.38$ in the spectrum of Q2138-4427 has at least one visible damped wing in the velocity profile (see Fig. 11) implying a column density N(H I) $\gtrsim 10^{19}$ cm^{-2}. Unfortunately, the spectra of Q2139-4433

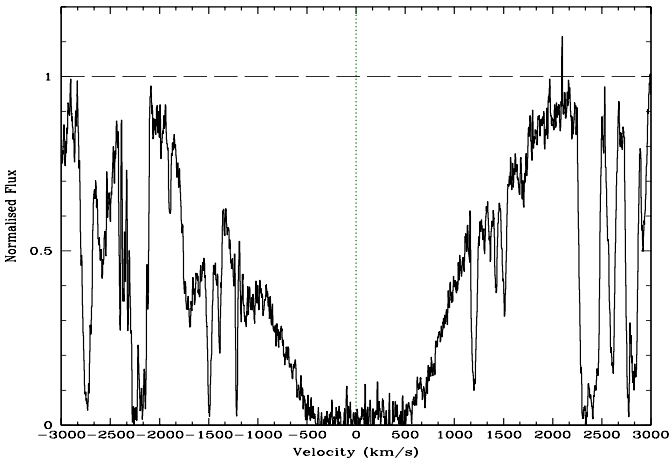

Fig. 11. Q2138-4427: H I Lyman-α absorption line at $z_a = 2.38279$.

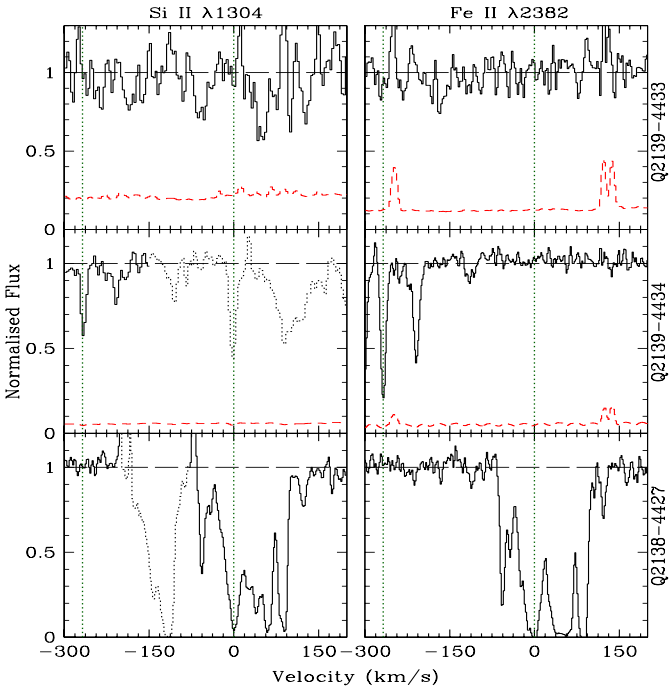

Fig. 12. $z \sim 2.38$ – coincident absorption systems in the spectra of Q2139-4434 (mid panels) and Q2138-4427 (bottom panels), with a transverse separation of $\sim 9\ h^{-1}$ Mpc. The left panels show the Si II λ 1304 transition and the right panels show the Fe II λ 2382 one. In the top row, the corresponding regions in the spectrum of Q2139-4433 are plotted. At this redshift, the separation between the LOSs to Q2139-4433 and Q2139-4434 is $\sim 1\ h^{-1}$ Mpc and between Q2139-4433 and Q2138-4427 is $\sim 7.7\ h^{-1}$ Mpc. The origin of the velocity axes is set at $z_a = 2.38279$. The other vertical dotted line marks the position of the system in Q2139-4434 at $z_a = 2.37977$.

and Q2139-4434 do not cover the wavelength region where the corresponding H I Lyman-α lines should fall, while the spectrum of Q2138-4427 does not cover that of the C IV doublet at this redshift. In the low resolution spectrum of Q2139-4434 by Francis & Hewett (1993), an absorption line with equivalent width ~20 Å is present at this redshift, which would correspond to a Lyman-α line with $N(\mathrm{H\,I}) \sim 7 \times 10^{19}$ cm^{-2}. We do not detect C IV absorption at this redshift in the

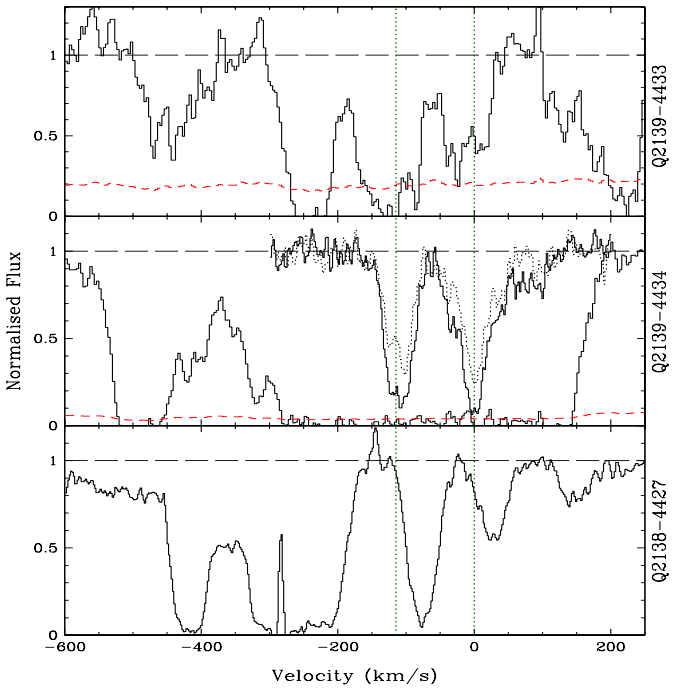

Fig. 13. $z \sim 2.73$ – LLS at $z_a \simeq 2.73557$ (origin of the velocity axes) in the spectrum of Q2139-4434 (middle panel). The H I Lyman-α absorption line is shown with superposed the lines of the C IV doublet. The other panels plot the corresponding H I Lyman-α line in the spectrum of Q2139-4433 (top) and of Q2138-4427 (bottom). No metal lines are associated to the latter two hydrogen absorptions. At this redshift, the transverse spatial separation between the LOSs to Q2139-4434 and Q2139-4433 is $\sim 1\ h^{-1}$ Mpc, between Q2139-4434 and Q2138-4427 is $\sim 9\ h^{-1}$ Mpc and between Q2139-4433 and Q2138-4427 is $\sim 8\ h^{-1}$ Mpc.

spectra of Q2139-4433 and Q2139-4434 but we identify neutral and singly ionised transition lines (C II, O I, Si II and Fe II) with a simple two-component velocity profile in Q2139-4434. Figure 12 shows two coincident transitions in Q2138-4427 and Q2139-4434, they have a minimal velocity separation of around 150 km s^{-1}, while the two LOSs are at a transverse separation of $\sim 9\ h^{-1}$ Mpc.

8) $z \simeq 2.73$ – the system at $z_a \simeq 2.73557$ in the spectrum of Q2139-4434 is again a candidate LLS on the ground of the observed ionic transitions. No metal lines are detected within ~3000 km s^{-1} of this absorption redshift along the LOS of Q2139-4433 and of Q2138-4427. On the other hand, the velocity profile of the observed H I Lyman-α absorptions follows that of the C IV absorption associated to the LLS (see Fig. 13). Unfortunately, we cannot disentangle the velocity structure of the LLS Lyman-α absorption since our spectrum does not extend to the region where the higher lines in the Lyman series are located.

9) $z \simeq 2.85$ – the DLAS at $z_a \simeq 2.85$ in the spectrum of Q2138-4427 coincides with a complex H I Lyman-α absorption in the spectrum of Q2139-4434, with no detectable associated metal transitions. On the other hand, we identify a saturated Lyman-α absorption ($W_r \simeq 1$ Å) and a C IV doublet at $z_a \simeq 2.85262$ in the spectrum of Q2139-4433 (see Fig. 14), partially superposing

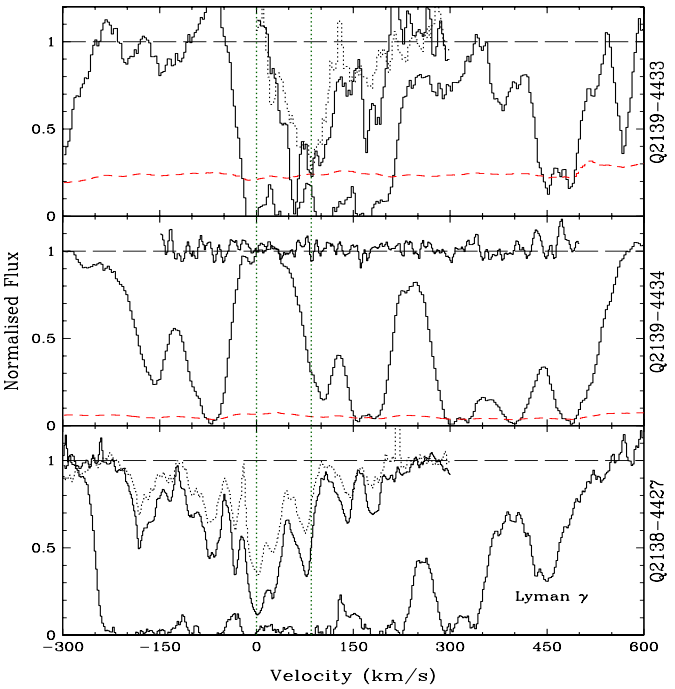

Fig. 14. $z \sim 2.85$ – coincident absorption systems in the spectra of Q2139-4433 (top panel), Q2139-4434 (middle panel) and Q2138-4427 (bottom panel). The H I Lyman-α transitions are shown in the top and mid row and the H I Lyman-γ corresponding to the DLAS in the spectrum of Q2138-4427 is in the bottom row. Overplotted are the corresponding C IV doublets, no metal absorption is observed in the spectrum of Q2139-4434. The dotted vertical lines mark the position of the main components in C IV at $z_a = 2.85153$ (origin of velocity axes) and at $z_a = 2.85262$. The transverse spatial separations between the three LOSs are about the same as those reported in the caption of Fig. 13.

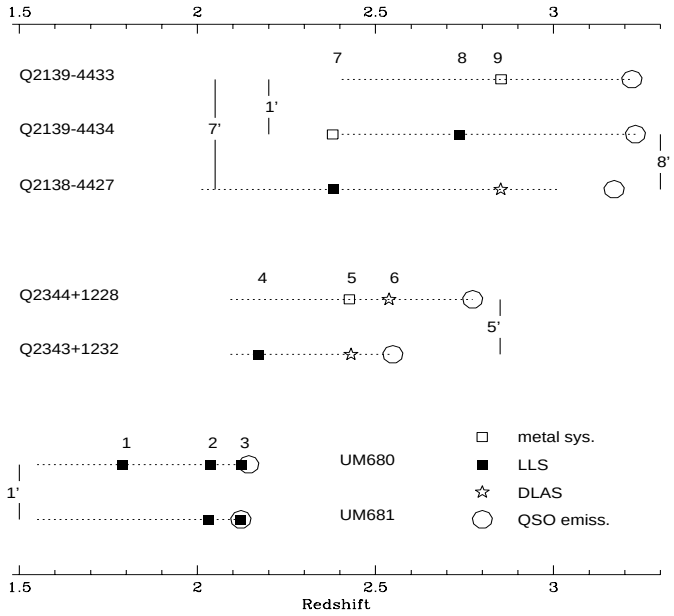

Fig. 15. Summary of the observed coincidences as a function of redshift. The dotted lines mark the redshift range of the observed Lyman-α forests. The angular separations of the quasars are reported between the solid vertical lines. The symbols are: open square for metal systems, solid square for LLS with $2\times10^{17} < N(\mathrm{HI}) < 2\times10^{20}$ cm^{-2} and star for DLAS with $N(\mathrm{HI}) > 2\times10^{20}$ cm^{-2}. The big open circles mark the emission redshift of the quasars.

in redshift upon the C IV absorption associated to the DLAS. The transverse spatial separation between the two LOSs at this redshift is $\sim 9\ h^{-1}$ Mpc.

This correlation could be interpreted as due to a gaseous structure perpendicular to the LOSs and extending over several Mpc in the direction defined by the three quasars.

5. Discussion

The expected number of DLAS ($N(\mathrm{H\,I}) > 2\times10^{20}$ cm^{-2}) and LLS ($2\times10^{17} < N(\mathrm{H\,I}) < 2\times10^{20}$ cm^{-2}) in the redshift interval covered by our 7 spectra as computed from their number density as a function of redshift – $N(z)_{\mathrm{DLAS}} \simeq 0.055(1+z)^{1.11}$, $N(z)_{\mathrm{LLS}} \simeq 0.27(1+z)^{1.55}$ (Storrie-Lombardi & Wolfe 2000)– is of 1 and 9, respectively. We detect 3 DLASs and 8 LLSs indicating that our lines of sight are not strongly biased toward an overabundance of high column density systems.

The investigation of the nearby lines of sight at the redshift of each of the previous systems, gives the following results. Of the three DLASs: 2 coincide with metal systems with C IV rest equivalent width $W_r(\lambda1548) > 0.5$ Å, and 1 is at less than 1000 km s^{-1} from the emission redshift of the paired QSO, which in turn is marking the presence of a high matter density peak (see Ellison et al. 2001). The transverse spatial separation over which these coincidences happen varies between ∼5 and 9 h^{-1} Mpc.

As for the 8 LLSs: 4 of them form two coinciding pairs at $z_a \sim 2.03$ and 2.12 in the spectra of UM680 and UM681, their transverse spatial separations are ∼920 and 940 h^{-1} kpc, respectively. The LLS at $z_a \sim 2.38$ in the spectrum of Q2138-4427 shows a coinciding metal system in the spectrum of Q2139-4434 at a transverse spatial separation ∼9 h^{-1} Mpc. However, only low-ionisation transitions are observed and no C IV. Furthermore, the H I Lyman-α of the latter system is outside our spectral range . The remaining 3 Lyman limit systems have corresponding Lyman-α absorptions without associated metals within 3000 km s^{-1}.

In summary, we measure a coincidence within 1000 km s^{-1} between high density systems, in 5 cases out of 10. We exclude the coincidence at $z \sim 2.38$ in the triplet, since it was not possible to determine the H I column density of the metal system. Figure 15 shows a pictorial description of the observed coincidences as a function of redshift; while in Table 4 we report the main properties of the matching absorption systems.

In order to approximately compute the significance of our result, we consider the number density of C IV systems with rest equivalent width $W_r > 0.3$ Å as a function of redshift (Steidel 1990). The chance probability (in the hypothesis of null clustering) to detect a C IV absorption line within 1000 km s^{-1}, between $z = 2$ and 3, is $\mathcal{P}_{\mathrm{exp}} \simeq 0.004$. If we assume that a binomial random process rules the detection or the non-detection of a coincidence, the *a posteriori* probability in the studied case is $<2.5\times10^{-10}$. The clustering signal is indeed highly significant.

Table 4. Summary of observed coincidences.

Objects	Ident.	Redshift[a]	Δs^b (h^{-1} Mpc)	$\Delta v^c_{\rm min}$ (km s^{-1})	log N(H I)	$W_{\rm r}(\lambda 1548)$ Å	log N(Fe II)
	1	1.7874	0.87		13.8	out	<11.8
		1.78865		>3000	19.0	out	14.5
UM680	2	2.0352	0.92	300	>18	0.4[d]	12.8
UM681		2.03215			>18	0.7[d]	13.4
	3	2.12312	0.94	100 (Si II)	>17.3	0.5	<12.7
		2.12209			>17.3	0.44	<12.6
	4	2.17115	5	>3000	>17.3	0.34	13.1
		2.167				<0.01	<11.8
Q2343+1232	5	2.43125	5.3	110 (Si IV)	20.35	1.1[e]	14.7
Q2344+1228		2.4271			>15.9	0.7[e]	<12.5
	6	2.549[f]	5.3				
		2.53788			20.4	out	14.1
	7	out	1			<0.014	<12.3
		2.37977	9	150 (Fe II)	20	<0.008	13.4
		2.38279	8		>19	out	e.w. 1.2[h]
Q2139-4433	8	2.73258			16.5	<0.03	<12.9
Q2139-4434		2.73557		>3000	>17.3	0.6	13
Q2138-4427[g]		2.7323				<0.005	<11.9
	9	2.85262		0 (C IV)		0.5	<13
		2.85378			14.8	<0.007	<12.6
		2.85153			20.9	0.8	e.w. 0.2[h]

[a] The reported redshifts correspond to the main component of the associated metal absorption, if present; or to the strongest H I Lyman-α absorption closer to the redshift of the high density system.
[b] Transverse spatial separation between the lines of sight; in the case of the triplet it refers to the distance to the following object in the list.
[c] Minimal velocity separation between metal absorption lines of the same ionic species in the coupled lines of sight.
[d] C IV λ 1548 rest equivalent width from Shaver & Robertson (1983).
[e] C IV λ 1548 rest equivalent width from Sargent (1987).
[f] Emission redshift of the paired QSO.
[g] Precise column density determination for the metal lines in the spectrum of Q2138-4427 will be reported by Ledoux et al. (in preparation).
[h] Rest equivalent width in Å.

Going back to our sample, the two coincidences in the spectra of UM680, UM681 at $\sim$1 h^{-1} Mpc are closely related to the emitting quasars. As recently claimed for associated absorption lines (e.g. Srianand & Petitjean 2000; de Kool et al. 2001; Hamann et al. 2001), the observed absorption systems could arise in gas expelled by a galactic "superwind" in a luminous starburst associated with the formation of the quasar itself. Superwinds contain cool dense clouds which justify the presence of low ionisation lines, embedded in a hot ($\sim 10^7$ K) X-ray-emitting plasma (see Heckman et al. 1996, and references therein). In low redshift galaxies, outflow velocities of 10^2–10^3 km s^{-1} and column densities $N(H) \sim$ few $\times 10^{21}$ cm^{-2} have been measured which are consistent with the observed values.

The remaining three coincident systems involve DLASs and are characterized by larger QSO pair separations. Damped systems at high redshifts are thought to arise in large disks (e.g. Wolfe 1995) or in multiple protogalactic clumps (Haehnelt et al. 1998; Ledoux et al. 1998; McDonald & Miralda-Escudé 1999). In either case they trace high matter density peaks and they are possibly associated with Lyman-break galaxies (Møller et al. 2002). The representation of these kind of objects in hydrodynamical simulations (e.g. Jenkins et al. 1998; Cen 1998) shows that they lie in knots of $\sim$1 h^{-1} Mpc scale from which filaments several Mpc in length depart in a spider-like structure. Star formation takes place in the central condensation but also in some denser blobs of matter along the filaments. The correlation on large scales observed around the DLAS in our sample finds a likely explanation in this scenario (see the discussion in Francis et al. 2001b). For comparison, Lyman break galaxies at $z \sim 3$, which are thought to have masses $M \sim 10^{11}\ M_\odot$, show correlation lengths $r_0 \sim 2\ h^{-1}$ Mpc

(Giavalisco et al. 1998; Porciani & Giavalisco 2001; Arnouts et al. 2002).

6. Conclusions

We have analysed new, high resolution UVES spectra of two QSO pairs and a QSO triplet (refer to Table 1 and Sect. 2) focussing mainly on the clustering properties of high matter density peaks, traced by LLS ($2 \times 10^{17} < N(\mathrm{H\,I})/\mathrm{cm}^{-2} < 2 \times 10^{20}$) and DLAS ($N(\mathrm{H\,I}) > 2 \times 10^{20}$ cm^{-2}). The observed number of DLAS and LLS in the considered lines of sight is in good agreement with the expected value.
The relevant conclusions are the following:

1. in 4 cases out of 10 there is a metal system with C IV rest equivalent width $W_\mathrm{r} > 0.5$ Å, in the paired line of sight within 1000 km s^{-1} of the redshift of the considered high column density absorption system. In 1 case, a DLAS matches the emitting QSO in the paired line of sight;
2. the correlation signal is highly significant in spite of the small sample. The gas giving rise to the coincidences close to the emission redshift of the QSOs (# 2 and 3 in Fig. 15) could be due to a starburst-driven galactic superwind. In the other cases (# 5, 6 and 9), involving DLASs, the gas could be in coherent filamentary or sheet-like structures of several Mpc, the possible ancestors of present-day rich clusters;
3. we measure the chemical abundance ratios in two DLAS and a sub-DLAS. In particular, we estimate the ratios C/Fe, O/Fe and Si/Fe for the DLAS at $z \sim 2.53788$ in the spectrum of Q2344+1228. The abundance ratios of these elements are consistent with solar values or very small enhancement at a variance with what is observed for halo stars at the same metallicity in the Milky Way.

Acknowledgements. V.D. is supported by a Marie Curie individual fellowship from the European Commission under the programme "Improving Human Research Potential and the Socio-Economic Knowledge Base" (Contract No. HPMF-CT-1999-00029). This work was supported in part by the European Community RTN network "The Physics of the Intergalactic Medium". It is a pleasure to thank C. Ledoux for the UVES spectrum of Q2138-4427.

References

Arnouts, S., Moscardini, L., Vanzella, E., et al. 2002, MNRAS, 329, 355
Ballester, P., Modigliani, A., Boitquin, O., et al. 2000, ESO The Messenger, 101, 31
Bergeron, J., & Boissé, P. 1991, A&A, 243, 344
Bergeron, J., Cristiani, S., & Shaver, P. 1992, A&A, 257, 417
Bergeron, J., & Stasińska, G. 1986 A&A, 169, 1
Bergeson, S. D., Mullman, K. L., Wickliffe, et al. 1996, ApJ, 464, 1044
Bergeson, S. D., Mullman, K. L., & Lawler, J. E. 1994, ApJ, 435, L157
Cen, R., Miralda-Escudé, J., Ostriker, J. P., & Rauch, M. 1994, ApJ, 437, L9
Cen, R. 1998, ApJ, 509, 16
Centurión, M., Bonifacio, P., Molaro, P., & Vladilo, G. 1998, ApJ, 509, 620
Chiappini, C., Matteucci, F., Beers, T. C., & Nomoto, K. 1999, ApJ, 515, 226
Cristiani, S., D'Odorico, S., D'Odorico, V., Fontana, A., Giallongo, E., & Savaglio, S. 1997, MNRAS, 285, 209
Dekker, H., D'Odorico, S., Kaufer, A., et al. 2000, in Optical and IR Telescope Instrumentation and Detectors, ed. M. Iye, & A. F. Moorwood, Proc. SPIE, 4008, 534-545
Dessauges-Zavadsky, M., D'Odorico, S., McMahon, R. G., et al. 2001, A&A, 370, 426
D'Odorico, V., Cristiani, S., D'Odorico, S., et al. 1998, A&A, 339, 678
D'Odorico, V., & Petitjean, P. 2001, A&A, 370, 729
Ellison, S. L., Pettini, M., Steidel, C. C., & Shapley, A. 2001, ApJ, 549, 770
Ferland, G. J. 1997, Hazy, a brief introduction to Cloudy 94.00 `http://www.pa.uky.edu/gary/cloudy`
Fontana, A., & Ballester, P. 1995, ESO The Messenger, 80, 37
Francis, P. J., & Hewett, P. C. 1993, AJ, 105, 1633
Francis, P. J., Williger, G. M., Collins, N. R., et al. 2001a, ApJ, 554, 1001
Francis, P. J., Wilson, G. M., & Woodgate, B. E. 2001b, PASA, 18, 64
Francis, P. J., Woodgate, B. E., & Danks, A. C. 1997, ApJ, 482, L25
Francis, P. J., Woodgate, B. E., Warren, S. J., et al. 1996, ApJ, 457, 490
Giavalisco, M., Steidel, C. C., Adelberger, K. L., et al. 1998, ApJ, 503, 543
Guillemin, P., & Bergeron, J. 1997, A&A, 328, 499
Grevesse, N., & Anders, E. 1989, in Cosmic Abundances of Matter, ed. C. J. Waddington, AIP Conf. Proc., 183 (New York: AIP), 1
Grevesse, N., & Noels, A. 1993, in Origin and Evolution of the Elements, ed. N. Prantzos, E. Vangioni-Flam, & M. Cassé (Cambridge Univ. Press), 15
Haehnelt, M. G., Steinmetz, M., & Rauch, M. 1998, ApJ, 495, 647
Hamann, F. W., Barlow, T. A., Chaffee, F. C., Foltz, C. B., & Weymann, R. J. 2001, ApJ, 550, 142
Hawkins, M. R. S., & Véron, P. 1996, MNRAS, 281, 348
Heckman, T. M., Dahlem, M., Eales, S. A., Fabbiano, G., & Weaver, K. 1996, ApJ, 457, 616
Hernquist, L., Katz, N., Weinberg, D., & Miralda-Escudé, J. 1996, ApJ, 457, L51
Jenkins, A., Frenk, C. S., Pearce, F. R., et al. 1998, ApJ, 499, 20
Katz, N., Weinberg, D. H., Hernquist, L., & Miralda-Escudé, J. 1996, ApJ, 457, L57
Kim, T.-S., Cristiani, S., & D'Odorico, S. 2001, A&A, 373, 757
de Kool, M., Arav, N., Becker, R. H., et al. 2001, ApJ, 548, 609
Le Brun, V., Bergeron, J., Boissé, P., & Deharveng, J. M. 1997, A&A, 321, 733
Ledoux, C., Petitjean, P., Bergeron, J., et al. 1998, A&A, 337, 51
Lu, L., Sargent, W. L. W., & Barlow, T. A. 1998, AJ, 115, 162
Madau, P., Haardt, F., & Rees, M. J. 1999, ApJ, 514, 648
Mar, D. P., & Bailey, G. 1995, Proc. Astron. Soc. Aust., 12, 239
McDonald, P., & Miralda-Escudé, J. 1999, ApJ, 519, 486
Miralda-Escudé, J., Cen, R., Ostriker, J. P., & Rauch, M. 1996, ApJ, 471, 582
Molaro, P., Bonifacio, P., Centurión, M., et al. 2000, ApJ, 541, 54
Møller, P., Warren, S. J., Fall, S. M., et al. 2002, ApJ, accepted [`astro-ph/0203361`]
Petitjean, P., Mücket, J. P., & Kates, R. E. 1995, A&A, 295, L12
Porciani, C., & Giavalisco, M. 2002, ApJ, 565, 24
Prochaska, J. X., & Wolfe, A. M. 2002, ApJ, 566, 68
Prochaska, J. X., & Wolfe, A. M. 1998, ApJ, 507, 113
Prochaska, J. X., Wolfe, A. M., Tytler, D., et al. 2001, ApJS, 137, 21
Raassen, A. J. J., & Uylings, P. H. M. 1998, A&A, 340, 300

Rauch, M., Miralda-Escudé, J., Sargent, W. L. W., et al. 1997, ApJ, 489, 7
Sargent, W. L. W. 1987, in QSO Absorption Lines: Probing the Universe, ed. J. C. Blades, D. Turnshek, & C. A. Norman (Cambridge University Press), 8
Sargent, W. L. W., Boksenberg, A., & Steidel, C. C. 1988, ApJS, 68, 539
Shaver, P. A., & Robertson, J. G. 1983 ApJ, 268, L57
Srianand, R., & Petitjean, P. 2000, A&A, 357, 414
Steidel, C. C. 1990, ApJS, 72, 1
Steidel, C. C., Sargent, W. L., & Boksenberg, A. 1988, ApJ, 333, L5
Steidel, C. C., Dickinson, M., & Persson, E. 1994, ApJ, 437, L75
Storrie-Lombardi, L. J., & Wolfe, A. M. 2000, ApJ, 543, 552
Theuns, T., Leonard, A. P. B., & Efstathiou, G. 1998, MNRAS, 297, L79
Tomkin, J., Woolf, V. M., & Lambert, D. L. 1995, AJ, 109, 2204
Tytler, D., & Fan, X.-M. 1992, ApJS, 79, 1
Verner, D. A., et al. 1994, A&AS, 108, 78
Viegas, S. M. 1995, MNRAS, 276, 268
Weymann, R. J., Williams, R. E., Petersen, B. M., et al. 1979, ApJ, 218, 619
Wolfe, A. M. 1993, ApJ, 402, 411
Wolfe, A. M. 1995, ASP Conf. Ser., 80, ed. A. Ferrara, C. F. McKee, C. Heiles, & P. R. Shapiro, 478
Wolfe, A. M., Lanzetta, K. M., Foltz, C. B., et al. 1995, ApJ, 454, 698
Wolfe, A. M., Turnshek, D. A., Lanzetta, K. M., & Oke, J. B. 1992, ApJ, 385, 151
Zhang, Y., Anninos, P., & Norman, M. L. 1995, ApJ, 453, L57